DEUTSCHES ELEKTRONEN-SYNCHROTRON

DESY 93-127
September 1993

Hodoscope Read-Out with Space-Time Mapping through an Optical Pipeline

A. Bamberger, E. Böhler, W. Kröger, S. Söldner-Rembold
Albert-Ludwigs-Universität, Freiburg i.Br.

ISSN 0418-9833

NOTKESTRASSE 85 - 22603 HAMBURG

To be sure that your preprints are promptly included in the
HIGH ENERGY PHYSICS INDEX,
send them to (if possible by air mail):

DESY **Bibliothek** **Notkestraße 85** **22603 Hamburg** **Germany**	**DESY-IfH** **Bibliothek** **Platanenallee 6** **15738 Zeuthen** **Germany**

DESY 93-127
September 1993

ISSN 0418-9833

Hodoscope Read-Out with Space-Time Mapping through an Optical Pipeline

A. Bamberger, E. Böhler,
W. Kröger, S. Söldner-Rembold

Albert-Ludwigs-Universität, Freiburg i. Br. , Germany

Abstract

This note describes a new read-out scheme for fine grained hodoscopes with possible applications for a Small Angle Rear Tracking Detector (SRTD) or a presampler in front of the ZEUS Uranium Calorimeter. Several hodoscope strips are read out by one phototube using optical fibres of different lengths. Optical delays of equal increments ensure a linear mapping of the space coordinate onto the time coordinate. A first prototype has been built and first test measurements are being presented.
In addition, Monte Carlo simulations were performed to study the effects of showering electrons on the position resolution of the detector.
The results of the test measurements, especially those related to the properties of the light guides, and the results of the simulation are of general importance for the SRTD design beyond the optical delay read-out scheme presented here.

Contents

1 Introduction and Motivation

This note is based on the proposal to build a Small Angle Rear Tracking Detector (SRTD) for the ZEUS experiment [1]. This new detector will be placed around the beam pipe in front of the Rear Calorimeter (RCAL) in order to to improve the reconstruction of scattered electrons at low x and moderate Q^2 [1]. This kinematic regime is of special interest for the measurement of the parton distributions at low Bjorken x [2].
The main tasks of the SRTD will be:

- To recognize whether electrons have showered in the material between the interaction point and the RCAL in order to correct for the energy loss.
- To improve the measurement of the position and the scattering angle of the electron.
- To provide additional timing information in order to reject upstream interactions in the trigger and in order to trigger on low x events at moderate Q^2.

Neglecting the electron mass, the squared four momentum transfer Q^2 is given by $Q^2 = 2EE'(1 + \cos\Theta_e)$, where E and E' are the energies of the incoming and the scattered electron, respectively, and Θ_e is the electron scattering angle measured in the laboratory system with respect to the proton axis. In order to obtain equal contributions to the Q^2 resolution from the measurement of the energy E' in the RCAL ($\sigma(E')/E' = 0.17/\sqrt{E'}$, E' in GeV) and the position measurement in the SRTD, the spatial resolution should be in the order of 5 mm assuming $E' = 17$ GeV and $\Theta_e = 170^0$. A small error on the position measurement will also improve the measurement of the scaling variable $x = Q^2/2M\nu$ (M is the proton rest mass and ν is the energy transfer).
Our proposal is therefore aimed at improving the spatial resolution of the SRTD by increasing the granularity of the SRTD, which currently has a strip width of 10 mm, without increasing the number of read-out channels. This is accomplished by a linear mapping of the space coordinate onto the time coordinate using optical delays. The idea is sketched in figure 1.1. Several strips of the hodoscope will be read out by one phototube. This greatly reduces the number of channels necessary. Of course, depending on the required position resolution it will also be possible to decrease the cost of the detector considerably by reducing the amount of money

needed for phototubes and read-out electronics (185 kDM in the SRTD proposal [1]).
A first version of this idea as a read-out scheme for a presampler was presented by D.Hanna [3], extending the delays beyond the repetition period of the beam crossings (96 ns), and in a proposal of the Freiburg group to the SRTD group [4]. For a Time of Flight (TOF) detector measuring heavy ion collisions at the LHC, optically multiplixed scintillation detectors were proposed recently by a group from the University of Catania [5].
An alternative approach is the use of position sensitive photomultipliers (PSPM) which has been tested recently [6]. An important drawback of this method is the high cost of the PSPM as well as the low fibre detection efficiency and the large cross talk.
The linear mapping preserves the first moment of the spatial distribution of deposited energy as long as the pulse height for a given light input is constant for different fibre bundles. This holds even if neighbouring pulses do overlap to some extent. As long as reconstruction algorithms do not make use of spatial cuts near the maximum of the distribution there is no loss of position accuracy. The second moment of a distribution can be extracted by unfolding if needed.
We want to emphasize that possible applications of the optical delay read-out scheme can also be imagined in connection with the ZEUS presampler or even with developments of LHC/SSC detectors.

2 Design Considerations

Since the basic design of the SRTD remains unchanged, we shall only discuss those points where the optical pipeline makes modifications necessary. The general layout of the modified detector is shown in fig. 1.1. The details will be described in this section. Many of the features could be transferred to other detector concepts (e. g. the presampler).

2.1 Scintillator and Optical Pipeline

Each scintillator is 4 mm thick. The granularity is given by the 4 mm width of the scintillator strip. The strips are either 24 cm or 44 cm long. They are grouped into 2 planes. This adds up to a total of 680 strips. The scintillators are being read out by bundles of fibres glued to one end of the scintillator. The fibres of 2

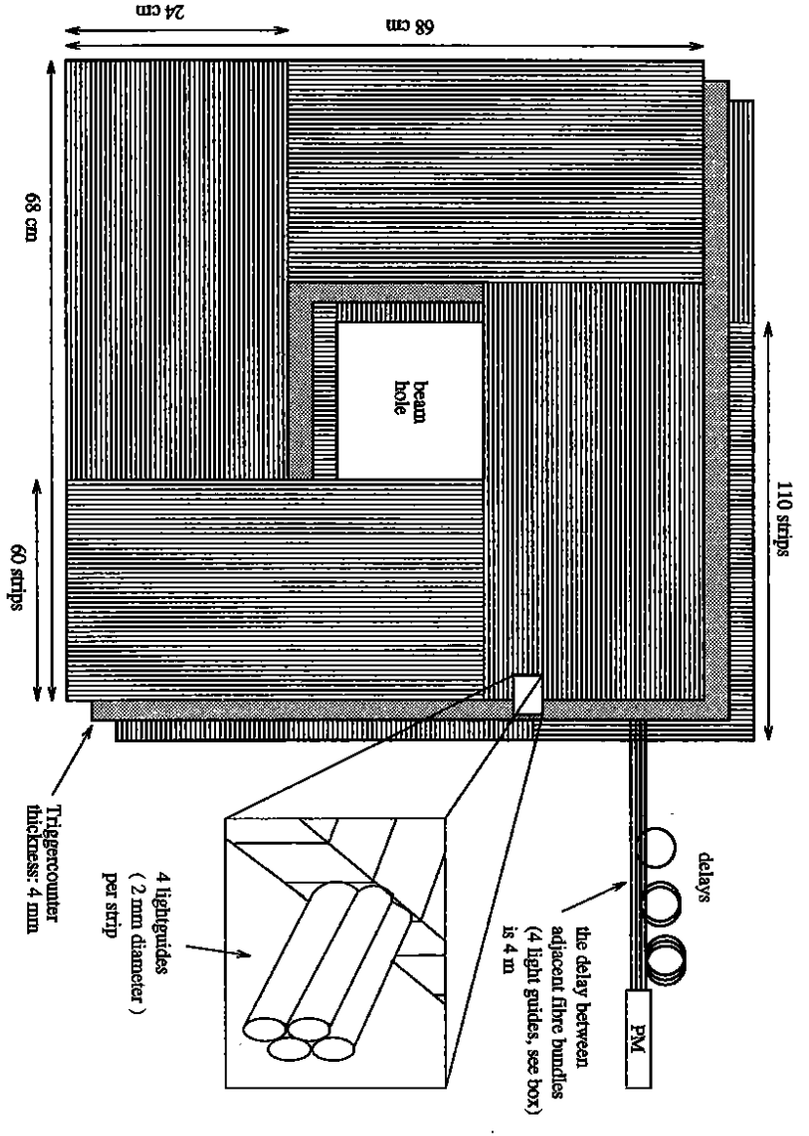

Figure 1.1: Possible design for a SRTD detector with optical delay lines. An additional plane is needed for timing and triggering information. Four strips will be read out by one PMT.

mm diameter are made by Mitsubishi [1] (Super Eska material, SK-80).
We assume that 20 cm fibre length correspond to 1 ns delay (i. e. the effective index of refraction equals 1.5). The pulses coming from the scintillator strips are delayed by fibres of different lengths. The difference in fibre length between adjacent strips is always 4 m corresponding to a step size of 20 ns. This means that 4 m of additional fibre have to be introduced for every additional channel which is read out by one PMT.
The number of strips which are being read out by one PMT has to be optimized by taking into account the complexity of the reconstruction, the length of the scintillation pulses, the light attenuation, the length of the fibres and the sampling frequency of the read-out. In addition, the maximum delay is chosen not to be longer than the HERA beam crossing period of 96 ns. Depending on the rate of ambiguities due to pile up, the maximum delay might be extended. We suggest to multiplex 4 strips with a delay of 20 ns between adjacent strips, adding up to a total delay of 60 ns, in view of the availability of a 100 MHz FADC from the CTD (chapter 2.3). A delay of 60 ns has been chosen to restrict the attenuation due to the fibre length (chapter 4.2).

2.2 Timing and Triggering

The SRTD is also being designed to improve the measurement of the event time in order to reject background from beam-gas events in the trigger and later on in the offline reconstruction. The timing resolution should be less than 1 ns.
In this scheme, the timing requirement is decoupled from the tracking by adding a third plane between the two planes of scintillator strips. This plane consists of 4 trigger counters, which cover the surface of 68×68 cm^2 excluding the beam hole. It is clear that the amplitude information can be measured for redundancy. The timing information from this counter would give the zero signal for the reconstruction of the delayed pulses. A thickness of 4 mm should be sufficient to have good light efficiency. The 4 mm thick trigger plane plus the 2×4 mm thick tracking planes increase the total thickness of the SRTD by 2 mm compared to the original SRTD design consisting of 2 planes of 5 mm thickness.
However, the complication of adding another plane for triggering and good timing is partially compensated by giving us the possibility to create a threefold coincidence of the three counter planes.

[1] Mitsubishi, Kennedydamm 19, 4000 Düsseldorf 30, Germany

2.3 Read-Out Chain

Each strip is coupled to a fibre bundle acting as light guide and delay line. In our case 4 fibres of 2 mm diameter are coupled to the scintillator. The fibres from 4 strips are bundled together.
It is vital for an optimal reconstruction of the pulses and the separation of neighbouring pulses to have sufficiently frequent sampling of the PMT pulse. A possible candidate for such a high sampling read-out scheme is the 100 MHz, 8 bit FADC used for the ZEUS Central Tracking Detector (CTD). It will be shown in chapter 3.5 that 8 bit are sufficient to obtain better than 10 % accuracy in the amplitude reconstruction using a linear FADC.
For 4 mm strip width, 172 read-out channels would be needed. The sampling time of 10 ns equals half the delay time. It should be coupled to the HERA clock. This guarantees that the read-out is in phase with the delayed signals. Depending on the pulse shape of the photomultiplier and scintillator signals it might be necessary to add shaping amplifiers to the read-out chain in order to have sufficient integration of the pulses for reconstructing the time and the amplitude of the pulses.

2.4 Homogeneity and Attenuation

The different lengths of the fibres and the inhomogeneity of the photocathode lead to different relative pulse heights for minimum ionizing particles (mips). A way of compensating the change in attenuation due to fibre length is the controlled bending of the shorter fibres. This will increase attenuation for the shorter fibres. It is also possible to achieve controlled light losses by coupling fibres with special connectors where the distance between the fibres can be varied [3]. Also the inhomogeneity of the photocathode can be used to partially compensate the light loss through the fibre.
A large attenuation over the longest fibres length would lead to unacceptable losses in the number of photoelectrons per mip. Measurements of the attenuation values will be presented later in this note (chapter 4.2).
Quartz fibres have lower attenuation than PMMA fibres. However, this alternative is ruled out, because of the additional cost of the quartz fibres.

2.5 Calibration

The remaining inhomogeneities must be corrected with a calibration system. A calibration with minimum ionizing particles (mips) has to be done.

To have good knowledge of the gain of each read-out chain from the scintillator through the light guide and the PMT requires calibrating the detector using a laser system. For such a laser system, at least one fibre from the laser has to be distributed to every scintillator strip. The light distribution system must allow to send light to different combinations of scintillator strips in order to test the response to overlapping pulses.

3 Simulation

A simplified simulation of the SRTD setup was performed in order to study the effect of passive material in front of the detector on the position resolution. It will be shown that a simple algorithm which averages over the position of all incoming shower particles does not yield sufficient accuracy. Furthermore, it will be investigated how the strip width influences the position resolution.
A high energy electron passing through an absorber will initiate an electromagnetic cascade. Therefore, there will be no single particle behind the absorber, but a number of electrons, positrons and photons. These particles do not longer follow the direction of the initial electron.
An electron which is scattered in the acceptance range of the SRTD ($162^0 < \Theta_e < 176^0$) has traversed between 1 and 7 radiation lengths of material (see figures 1 and 6 and the table in section 4 of reference [1]). Between 162 and about 173 degrees the dead material is mainly due to the VXD chambers. The number of radiation lengths X_0 can be estimated from the difference $d = 2.75$ cm of the inner and outer radius of the VXD material:

$$X/X_0 = d/(X_0 \cdot \sin(180 - \Theta_e)).$$

For aluminum ($X_0 = 8.9$ cm), one obtains between 1 and 2.5 radiation lengths. Electrons scattered close to the beam pipe traverse several flanges which can be described by 12 cm of iron corresponding to about 7 radiation lengths of material. Therefore the influence of 1, 2 and 6 X_0 thick aluminum absorbers was simulated. The simulation has been done using the ZEUS trigger Monte Carlo (MC) program (version T2) generating 30 GeV electrons impinging perpendicularly onto the aluminum plate. The simulation program contained an energy cut of 1 MeV. All electrons and positrons below this energy were not tracked. The cut of 1 MeV matches the maximum energy deposition of an electron or positron in the proposed hodoscope. The sensitivity of the energy cut on the number of charged particles

and on the position resolution will be discussed later.
For the simulation, the electromagnetic shower terminator, an option within the trigger Monte Carlo program which distributes the energy after a certain cut-off energy into pseudo-particles, was switched off. The terminator would reduce the number of charged particles leaving the aluminum plate by a factor of two, which is not realistic as will be shown below.

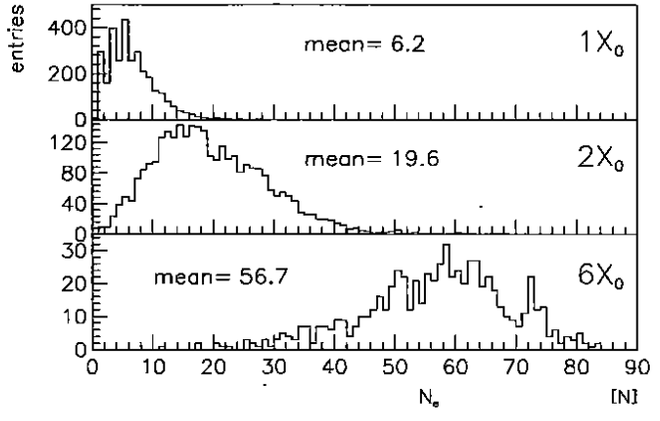

Figure 3.1: Number of electrons leaving the Al absorber for 1, 2 and 6 radiation lengths X_0. The initial electron energy is 30 GeV.

3.1 Charged Multiplicity

In general, many electrons, positrons and photons will leave the absorber, but rarely a single minimum ionizing particle, if a certain thickness of the absorber is exceeded.
The number of charged particles leaving the aluminum absorber of different thickness is shown in fig. 3.1 for electrons of 30 GeV initial energy. Behind 1 X_0, the multiplicity of charged particles is already large, and, correspondingly, the fraction of electrons passing the absorber unaffected is small. As an example, an electron having lost less than 1 GeV of its initial energy, occurs only to 0.3 %. In an absorber with a thickness corresponding to more than 2 X_0 all electrons start to shower.

For a detailed comparison with test beam results carried out at CERN, the response of a scintillator sheet of the same area as the aluminum plate positioned 2 cm behind the absorber was simulated. The scintillator signals in units of minimum ionising particles (mips) are shown in fig. 3.2. In this comparison the most probable energy loss (mop) was taken as being representative for a mip. This value has been determined by fitting a gaussian to the central peak. For a 1 (2) X_0 thick aluminum absorber, the mop value obtained from the data is 5.5 (19.9) and 5.6 (20.2) from the MC simulation. This is an good agreement with the measurements. The difference between the width of the distributions in MC and data for 0 X_0 is due to noise, which has not been simulated in the MC program. For 2 X_0, the tails towards higher multiplicities extend further in the MC simulation than in the testbeam data.
In conclusion the overall characteristics of the multiplicity of charged particles are correctly reproduced.

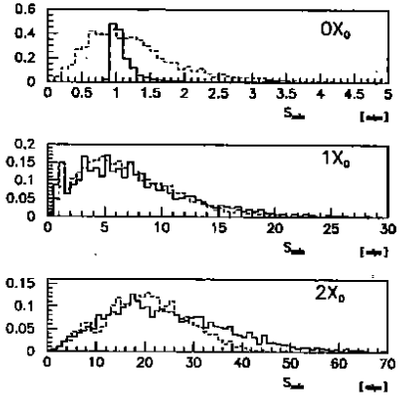

Figure 3.2: Scintillator signal in mips for 0, 1 and 2 X_0 Al absorber. Solid line: MC simulation; dashed line: testbeam data.

3.2 Lateral Shower Width

The spread S of the spatial distribution of charged particles at a distance d between the rear side of the aluminum absorber and the hodoscope plane has been estimated

by

$$S = \sqrt{\frac{1}{N}\sum_{i=1}^{N} d^2 \cdot \sin^2\theta_i} \approx d \cdot \sqrt{\frac{1}{N}\sum_{i=1}^{N}\theta_i^2} \approx d \cdot \sqrt{\langle\theta^2\rangle}.$$

N is the number of charged particles in an event. The distance between the absorber and the hodoscope is d. It is assumed that the spatial spread of charged particles at the rear face of the absorber is negligible.

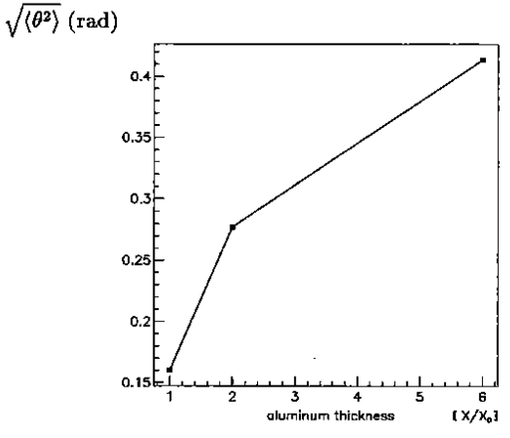

Figure 3.3: Mean angular spread $\sqrt{\langle\theta^2\rangle} = S/d$ for charged particles versus the aluminum absorber thickness. The distance between the absorber and hodoscope is d.

Fig. 3.3 shows the mean angular spread versus the absorber thickness in radiation lengths X_0. For 2 radiation lengths X_0 and $d = 100$ cm, the spread S is about 27 cm. This large spread is mainly due to the long tail in the distribution of polar angles θ of the charged particles, as shown in fig. 3.4.
The influence of the energy cut was investigated for an absorber thickness of 2 X_0. For an energy cut of 0.1 MeV, it was found that the changes on the number of charged particles and on the position resolution discussed in chapter 1.4 are negligible. However, for an energy cut of 10 MeV, the mean angular spread is reduced by about 30 % and for 100 MeV even by 90 %. In addition, the angular spread of low energy electrons might be influenced by the magnetic field. This effect was not simulated for this study.

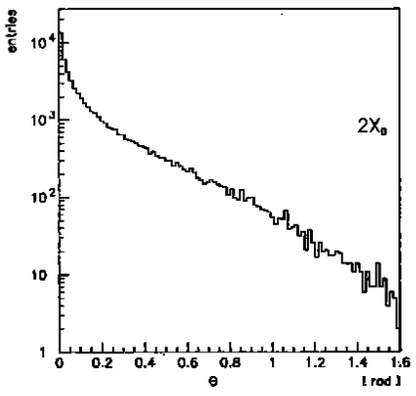

Figure 3.4: Distribution of the polar angles θ for electrons and positrons (MC simulation).

3.3 Mean Position

The x coordinate is defined as the direction perpendicular to the shower axis and parallel to the hodoscope (i. e. not in the ZEUS coordinate system). The segmentation of the hodoscope is in x direction. The mean position $\overline{x}$ was reconstructed by summing over all charged particles N

$$\overline{x} = \frac{1}{N}\sum_{i=1}^{N} x_i$$

where x_i is the position of the ith particle in the hodoscope plane. For all three radiation lengths X_0, the rms (root mean square) of the reconstructed mean position $\overline{x}$ is about 1.3 cm for a distance $d = 15$ cm between the absorber and the hodoscope plane. For $d = 100$ cm distance, the rms increases to about 8 cm as shown in fig. 3.5 where the reconstructed mean position $\overline{x}$ is plotted for an absorber of 2 X_0 and a hodoscope strip width of 4 mm.
If a gaussian is fitted to the peak as shown in fig. 3.5, the σ is smaller than the rms, but it is still 5 cm for a distance d of 100 cm. As in the case of the shower width, the large spread is due to particles emitted with large angles relative to the direction of the incident electron.

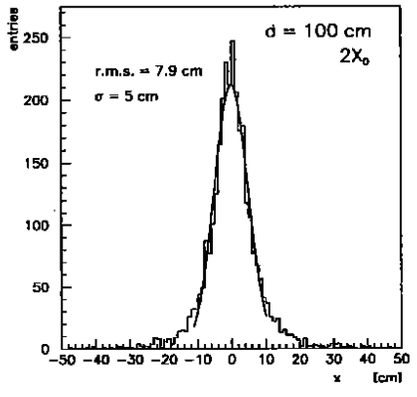

Figure 3.5: Mean position x. The position has been reconstructed by averaging over all charged particles.

3.4 Reconstruction Algorithm

For a hodoscope strip read-out, the position reconstruction was studied using the following method: A cluster was defined by the strip with the highest multiplicity and by adding all neighbour strips so that the width covered by all strips is about 3 cm. The reconstructed cluster position is the sum over the geometrical centers of the strips, each strip weighted by the number of charged particles passing the strip.
If there is an ambiguity, because there are more than one cluster, the position was reconstructed by averaging over the cluster positions.
The reconstructed x position of the incident electron is shown in fig. 3.6. The strip width b was 4 mm. A gaussian was fitted to the central peak. The σ of the gaussian is now 3.5–4 mm. However, there are large tails. These tails are due to spatially very asymmetric distributions of the charged shower particles and also due to events, where more than one cluster has been found. The position resolution may increase by using a more sophisticated reconstruction algorithm and after adding the information of the calorimeter and the HES (Hadron Electron Seperator) for the position reconstruction. This may also remove the tails.

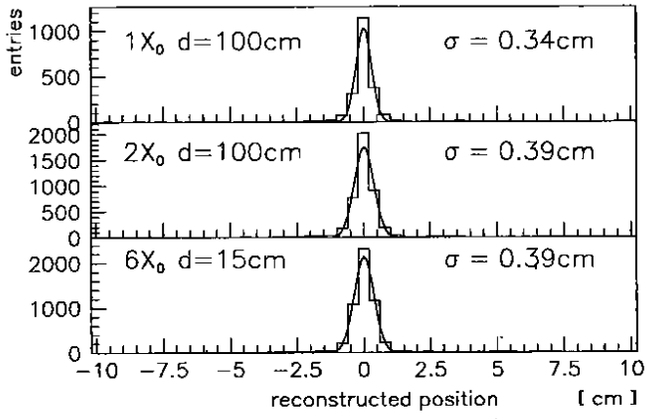

Figure 3.6: Mean reconstructed position x evaluated by the cluster method. The σ value is the result of a gaussian fit to the distribution. The electron was generated at $x = 0$.

The position resolution depends also on the strip width. This effect has been studied for strip widths b between 4 and 30 mm using the cluster method. A gaussian was fitted to the distributions even though the distributions are not exactly gaussian in shape due to long tails. The results are shown in fig. 3.7.
The position resolution above 15 mm is significantly worse than the resolution for smaller strips. A 4 mm strip width improves the position resolution only by a small amount ($< 10\%$) compared to a strip width of 10 mm. From this we conclude that the strip width should be in the range of 4–10 mm, where the best resolution is achieved.

3.5 Charged Particles per Strip

For the dynamic range of the readout chain, the multiplicity of charged particles is an important quantitiy.
The maximum number of charged particles per event passing a 4 mm strip of the hodoscope is shown in fig. 3.8. For the evaluation of an upper bound of the maximum number of charged particles, the distance between the absorber and the hodoscope was kept 15 cm for 2 X_0 and for 6 X_0, although the actual distance is

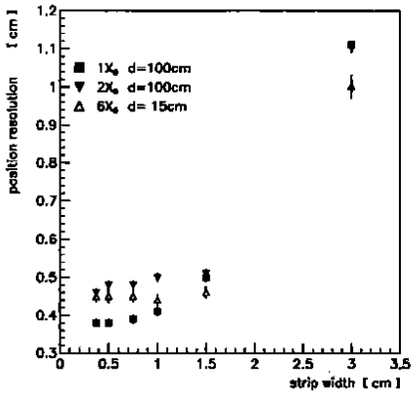

Figure 3.7: Position resolution σ versus the strip width b of the hodoscope. The resolution was determined by fitting a gaussian to the distribution of the mean reconstructed position.

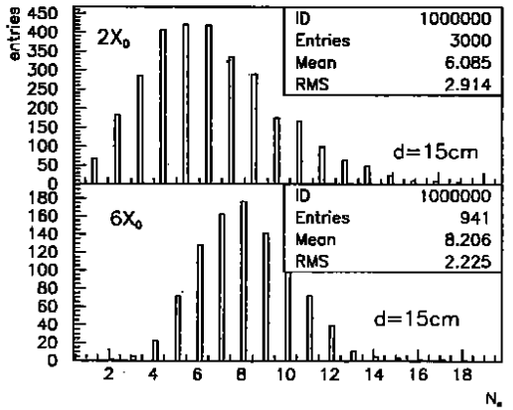

Figure 3.8: Maximum number of charged particles passing through a 4 mm strip.

100 cm for 2 X_0. The maximum number is about 15 particles. If the strip width increases, the maximum number of charged particles per strip also increases. For a hodoscope with 1 cm strip width, the maximum number of charged particles increases by about 30 %.
A multiplicity of 25 mips per strip would yield about 10 % accuracy in the amplitude reconstruction for a single mip using a linear 8 bit FADC (chapter 2.3).

4 Prototype Measurements

A first prototype was built at the University of Freiburg to test the concept of optical delay read-out. This prototype is scaled down in thickness and width by a factor of 2 compared to the device described in chapter 2.

4.1 Prototype Design

A conceptual drawing of the prototype design is shown in fig. 4.1. The 10 scintillator strips are 2×2 mm^2 thick and 20 cm long. The scintillator strips are of the type BCF-28 and were made by BICRON [2]. BCF-28 is a green-emitting, plastic scintillating fibre with a polystyrene core and PMMA cladding. According to the specifications the scintillation decay time is 12 ns, the scintillation efficiency (percentage of the electron's energy which is converted into light) is 1.6 %.
A bundle of 4 optical fibres, each fibre with a diameter of 1 mm, were glued to the end of every strip. All 4 fibres had the same length. The minimum length of the fibres was 3 m. For every strip 80 cm of fibre were added to delay the signal by 4 ns. The longest fibre was therefore 10.2 m long. For technical reasons, this delay is different from the delay of 20 ns which we propose for the SRTD optical delay line.
All fibres were bundled together on the photosensitive cathode of a XP1911 EMC tube. The signals were being read out with a 500 MHz sampling scope which was connected to a plotter.
The scintillator was excited by the UV-light of a Nitrogen laser. The light was transported through a light guide which was directly pointed to the open end of the scintillator strip. Part of the laser pulse was sent to a fast vacuum diode which was used to trigger the scope.
For a second test using a ^{106}Ru source, a blue scintillator strip of the same dimensions was positioned underneath the test counter and directly connected to a R580 (HAC) tube. The radioactive source was placed directly above the counter and the R580 tube was used to trigger the scope.

4.2 Attenuation of Light

The attenuation of light in the read-out fibres is of general importance for the SRTD design in order to estimate the number of photoelectrons which can be

[2] P. O. Box 564, 2400 An Alphen A/D Rijn, The Netherlands

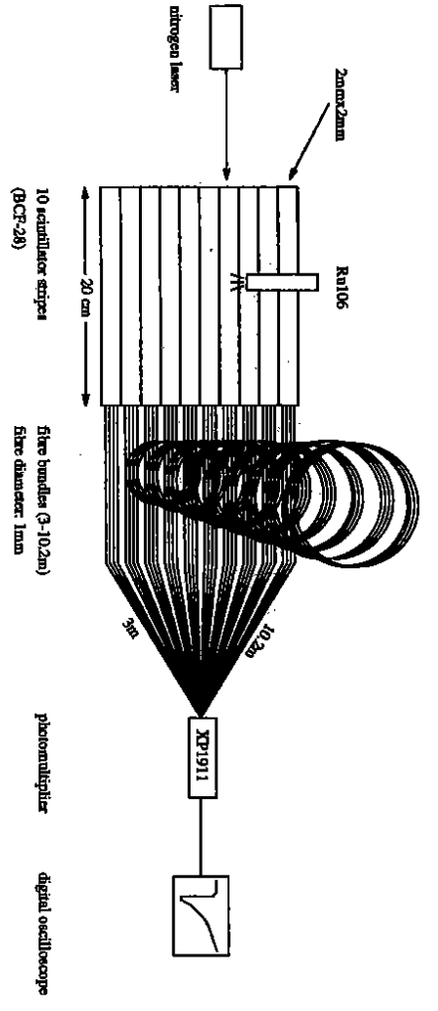

Figure 4.1: Conceptual drawing of the Freiburg prototype.

collected. For the SRTD protoptype measurement of the standard design [1], only 25 cm long fibres were used.

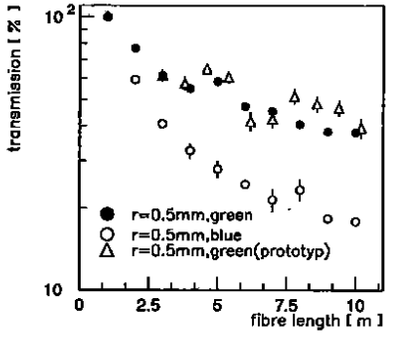

Figure 4.2: Light transmission versus fibre length measured for green and blue light using a halogen lamp.

We measured the attenuation of green and blue light in Mitsubishi fibres made of PMMA using light from a halogen lamp. The fibre diameter is 1 mm. The light output was measured with a photodiode. A 10 m fibre was cut in 1 m steps and the light output was measured. In between, the stability of the light source was monitored with fibre of fixed length. The data points shown in fig. 4.2 are normalized to the measurement of the diode current for the 1 m fibre (= 100%) and with respect to the values obtained for the monitor fibre. Plotted is the transmission which is defined as the percentage of light transmitted through the fibre with respect to the first measured point.
There seem to be two relevant length scales for the attenuation. In the first 3 m the attenuation is large compared to the region between 3 and 10 m. Similiar observations have been made by [7], where this effect has been attributed to a very good core-clad interface in the fibre, giving rise to a long attenuation length for the core light, and to imperfections at the clad-air (or clad-jacket) interface, which attenuate the clad light much faster. It should be stressed that for any practical device, the minimum fibre length is around 3 m. This means that only the larger attenuation lengths in the region beyond 3 m fibre length are of importance for the design of the optical delay line.
In general, the attenuation is much larger for blue light than for green light. The dB value was determined for a fibre length between 4 and 10 m. For green light it

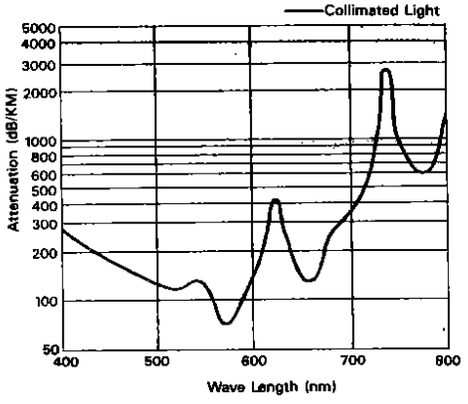

Figure 4.3: Attenuation measured in dB as a function of wavelength. Fibre type: Eska Extra (Mitsubishi). The plot has been copied from the Mitsubishi specifications.

is (330 ± 72) dB/km and for blue light (429 ± 138) dB/km. This is about a factor of 2-2.5 larger than the values quoted by Mitsubishi for a similar fibre type (Eska Extra, Fig. 4.3).
In addition, the attenuation was measured using the test setup. Pulsed laser light from a N_2 Laser was injected into the scintillator strips. The strips were read out by fibres of different length which are coupled to a single PMT. For such a measurement additional inhomogeneities are to be expected from the variation of the optical coupling of the fibres to the scintillator and to the photocathode of the PMT. Since the scintillator is emitting green light, we have to compare the measured attenuation values for the laser/PMT-setup with the green light from a halogen lamp (fig. 4.2). The minimum fibre length is 3 m for the laser/PMT-setup, therefore the attenuation values are normalized to this point. As expected the fluctuations are larger, but the slopes agree well. The measured attenuation is (257 ± 62) dB/km.
No significant difference is seen between the attenuation of fibres with different radii (r = 0.5 mm and r = 1 mm) in fig. 4.4. The measurement was done with blue light and the halogen lamp.
The number of photoelectrons (N_{pe}) which can be obtained with the test setup for one mip was estimated with the ^{106}Ru source. For the test setup this number is low ($N_{pe} \approx 1.5$) compared to the SRTD test setup at DESY ($N_{pe} \approx 20$, [1]). This can be understood by taking into account both, the reduction of the number of photoelectrons due different thickness of the scintillators (2 mm vs. 5 mm), different scintillation efficiencies (chapter 4.1) and the length of the fibres (only

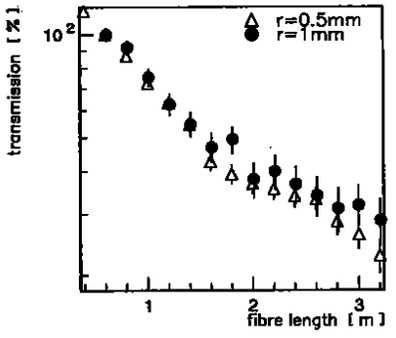

Figure 4.4: Transmission versus fibre length for fibres with radius $d = 1$ mm and $d = 2$ mm (blue light, halogen lamp).

25 cm for the SRTD test setup), and the increase of the number of photoelectrons due to the different attenuation for blue and green light.

4.3 Light Compensation and Fibre Bending

For the pulse reconstruction, the different attenuation values of the scintillator fibres due to different fibre lengths and due to the coupling of the fibres to the scintillators and the PMT should be compensated (chapter 2.4).
The compensation can be achieved by bending the fibres. The transmission depends on the bending radius and the number of loops. Again this was measured using the halogen lamp, but for blue light, only. In fig. 4.5a the transmission after one bending is plotted versus the bending radius R for fibres with radii r of 0.5 and 1 mm. 100 % corresponds to an unbent fibre. For a fibre with radius 0.5 mm practically no attenuation is observed for bending radii greater than 2 cm.
The transmission seems to depend only on the ratio R/r of the bending radius R and the fibre radius r. The transmission as a function of this ratio looks very similiar for both fibre types (fig. 4.5b).
Fig. 4.6 shows the transmission as a function of the number of loops for $r = 0.5$ mm fibres (fig. 4.6a) and for $r = 1$ mm fibres (fig. 4.6b). The biggest effect can be observed after the first loop, further bendings have little effect on the attenuation.
For the protoype the same mechanism was used to equalize the pulse heights for the ten scintillator strips. The bending was done with cylinders of 1 and 1.75 cm radius. With this method the signal height was equalized to better than 3 %

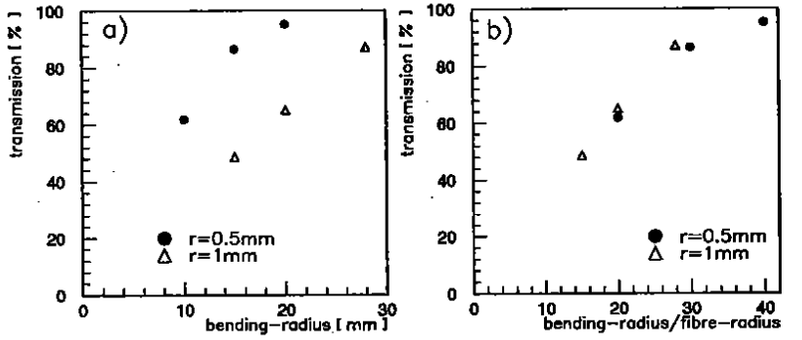

Figure 4.5: **a**: *Light transmission after one loop versus bending radius R measured for blue light using a halogen lamp and fibres of radius $r = 0.5$ and 1 mm.* **b**: *Light transmission versus the ratio R/r of the bending radius R and the fibre radius r.*

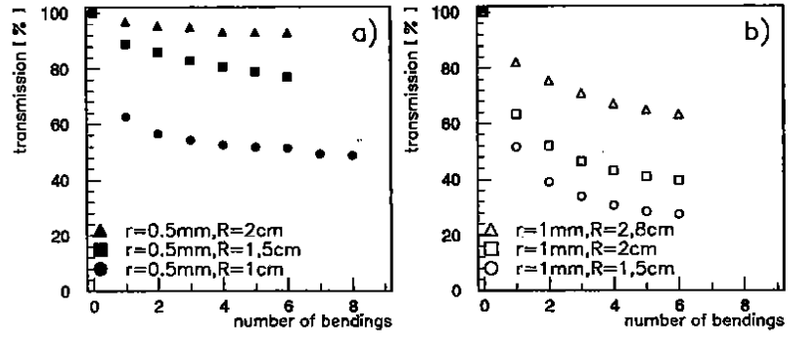

Figure 4.6: Light transmission versus the number of loops for different bending radii (1, 1.5 and 2 cm) measured with blue light using a halogen lamp. **a**: *fibre radius $r = 0.5$ mm;* **b**: *$r = 1$ mm.*

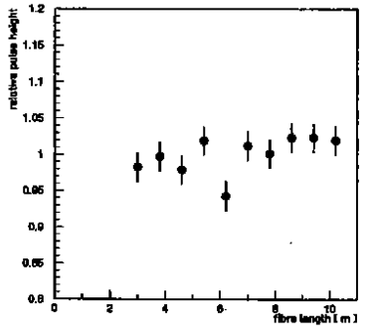

Figure 4.7: Transmission versus fibre length after compensating different attenuations and couplings by bending the fibres.

(fig. 4.7).
Bending fibres can lead to aging effects which were not studied here. A possible solution to this problem could be heating the fibres after bending in order to reduce stress. Alternative solutions like varying the distance between the fibres ends at the coupling (chapter 2.4) should also be considered.

5 Time Delay of Pulses

Fig. 5.1 shows a typical double pulse structure obtained with the N_2 laser for a simultaneous laser pulse which was injected in the first (3 m fibre) and last (10.2 m fibre) scintillation strip and measured by the PMT. The pulse heights are not compensated. The pulse length of 20–30 ns is due to the scintillator material and the PMT. For possible applications the length of the pulses can still be reduced by using different scintillator material and/or a faster PMT. This would reduce the overlap or 'cross talk' between the signals.
From the measured pulse shape of the blue scintillator it was estimated that the contribution of the tail of a pulse to the amplitude of the following pulse is about 4 %.
The relative time delay of all pulses was determined by injecting the laser light into the strips individually. The time with respect to the signal of the vacuum

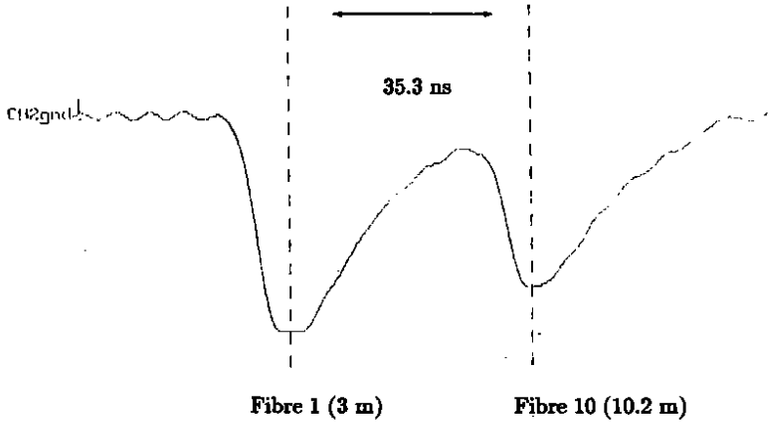

Figure 5.1: Two simultaneous laser pulses in the first and the last scintillator strip. The nominal time difference is 36 ns.

diode which was used for triggering was measured using the digital scope. The correlation between the time t_c calculated from the fibre length and the time t_m measured for the pulses has been plotted in fig. 5.2a and the deviation $t_m - t_c$ in fig 5.2b. The fluctuations can be explained by the precision of the oscilloscope.
The mean delay from one fibre to the next was obtained by averaging over all measurements. It is (3.9 ± 0.1) ns corresponding to a propagation speed of (0.69 ± 0.02) c.

6 Outlook

After collecting these first experiences, we plan to construct a second prototype in the next weeks. This prototype will be built with blue emitting scintillator to increase the output of photoelectrons. The time delay will be 20 ns as proposed. With this setup we hope to take data with a electron test beam at DESY in order to test the concept of optical delay lines under more realistic conditions and with higher statistics.

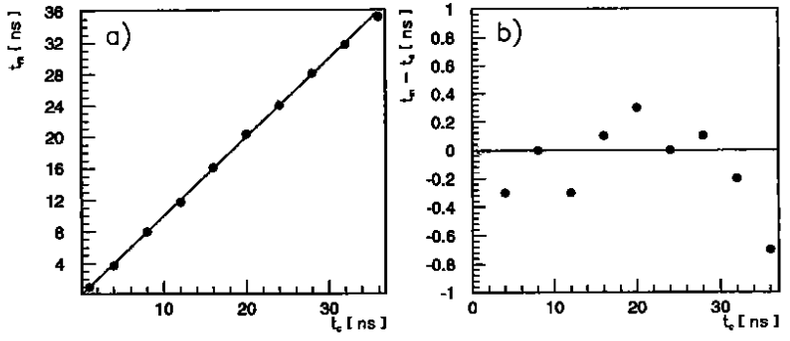

Figure 5.2: **a:** *Calculated time t_c from the fibre length versus the time measured t_m with a digital oscilloscope* **b:** *t_m-t_c versus t_c (no errors shown).*

7 Conclusions

We propose to read out hodoscopes like the Small Angle Rear Tracking Detector (SRTD) or the presampler for the ZEUS calorimeter using the principle of an optical pipeline. The signals from the scintillators are delayed in steps of 20 ns by optical fibres of different length. The central idea of this read-out scheme is a linear mapping of the space coordinate onto the time coordinate. The read-out would be done with a 100 MHz FADC.

With this method one can either reduce the number of read-out channels by a factor of 4 or improve the spatial segmentation. Applications of this read-out scheme can also be imagined for LHC and SSC detectors.

The position resolution of the hodoscope has been studied by a Monte Carlo simulation. The simulations shows that almost all electrons have started an electromagnetic shower in front of the SRTD counter, because of 1–6 X_0 of material between the interaction point and the SRTD. Because of the large fluctuations of the positions of the shower particles, special algorithms are needed to obtain a position resolution in the order of a few mm. The position resolution can be optimized by choosing a strip width below 10 mm.

A small prototype was built at Freiburg University. First results of the prototype measurements demonstrate the feasibility of such an optical delay line. The attenuation of blue light in the read-out fibres is about 429 dB/km corresponding to 70 % attenuation for total delays of 60 ns (12 m fibres). Different signal amplitudes

due to different fibre lengths and couplings were compensated to better than 3 % by bending the fibres. The number N_{pe} of photoelectrons per mip was estimated to be about 1.5. This number will have to be improved in a second prototype which will be built in the near future.

Acknowledgements:

We are very grateful to R. Klanner, H. Tiecke and D. Hanna for the careful reading of the manuscript and many important suggestions.

References:

[1] Proposal for a Small Angle Rear Track Detector for ZEUS, ZEUS-Note 93-016.
[2] Proceedings of the Workshop on Physics at HERA, Hamburg, October 29-30, 1991.
[3] D. Hanna, Optical Pipeline Readout of the ZEUS Presampler, November 10, 1992.
[4] Freiburg University, Small Angle Rear Tracker using Optical Pipe Line Delay, ZEUS internal note.
[5] R. Potenza et al., Proposal for Optically Multiplexed Scintillation Detectors for TOF, Univ. of Catania, September 22, 1992.
[6] J. Bähr et al., DESY 92-176, December 1992.
[7] C. M. Hawkes et al., NIM A292 (1990) 329–336.